

Early Anomaly Detection and Localization in Distribution Network: A Data-Driven Approach

Xin Shi¹, *Student Member, IEEE*, Robert Qiu^{1,2}, *Fellow, IEEE*, Xing He¹, *Member, IEEE*,
Zenan Ling¹, Haosen Yang¹, Lei Chu¹, *Student Member, IEEE*

Abstract—The measurement data collected from the supervisory control and data acquisition (SCADA) system installed in distribution network can reflect the operational state of the network effectively. In this paper, a random matrix theory (RMT) based approach is developed for early anomaly detection and localization by using the data. For every feeder in the distribution network, a corresponding data matrix is formed. Based on the Marchenko-Pastur Law for the empirical spectral analysis of covariance ‘signal+noise’ matrix, the linear eigenvalue statistics are introduced to indicate the anomaly, and the outliers and their corresponding eigenvectors are analyzed for locating the anomaly. As for the low observability feeders in the distribution network, an increasing data dimension algorithm is designed for the formulated low-dimensional matrices being more accurately analyzed. The developed approach can detect and localize the anomaly at an early stage, and it is robust to random disturbance and measurement error. Cases on Matpower simulation data and real SCADA data corroborate the feasibility of the approach.

Index Terms—early anomaly detection and localization, distribution network, SCADA data, random matrix theory, increasing data dimension

I. INTRODUCTION

THE distribution network is an important part of the power system, and its operating state is directly related to the safety of the entire system. One main factor that influences the operating state of the distribution network are the anomalies caused by overload, unbalanced three-phase voltage or current, system swing, etc. The anomalies, in general, may last for a period of time, but if can’t be detected and located in time, they will be likely to expand and even cause power failures or system black out. Therefore, it is important to realize anomaly detection and localization at an early stage for the safety analysis and decision making of control strategy. In practice, the anomaly usually generates complex, nonlinear and intermittent features with random magnitude [1], which makes it difficult for detecting and localizing them at an early stage. Meanwhile, with the increasing expansion of distribution network, it becomes more difficult for the model-based approaches to realize early anomaly detection and localization for the numerous branch lines and complex network topology.

Along the years, there have been significant deployments of online monitoring devices in power systems, which lies the foundation to enable a true monitoring, such as linear state estimation [2], dynamic state estimator [3] or fully measurements of all state variables [4]. The massive data collected from them can reflect the operational states of the system effectively, which stimulates the researches on data analytics for anomaly detection and localization. In [5], a novelty detection approach based on one-class support vector machines (SVMs) is developed for time-series data analysis. In [6], based on principal component analysis (PCA), the dimensionality of the phasor-measurement-unit (PMU) data is reduced for detecting the anomaly events in power systems at an early stage. In [7], a long short term memory (LSTM) network based approach is proposed for analyzing the time-series data. In [8], the PMU data is modeled and analyzed by applying the hypothesis test theory for multiple covariance matrix. In [9], a real-time anomaly detection and abnormal line identification approach is developed, which merges the early anomaly detection and localization functionalities. In [10], a density-based detection algorithm is proposed to detect local outliers, which can differentiate high-quality synchrophasor data from the low-quality one during system physical disturbance. In [11], a structured autoencoder network is designed for detecting abnormal behavior in manufacture systems.

Due to the massive data collected in a distribution network, the demand for theories capable of processing high-dimensional data has grown dramatically. The random matrix theory (RMT), introduced by Wishart in 1928 [12], is an important mathematical tool for statistical analysis of high-dimensional data. As for high-dimensional random matrices, the importance of the RMT for statistics comes from the fact that it may be used to correct traditional tests or estimators which fail in the ‘large p , large n ’ setting, where p is the number of parameters (dimensions) and n is the sample size. The RMT starts with asymptotic theorems on the distribution of eigenvalues or singular values of random matrices with certain assumptions, and eventually gives macroscopic quantity to indicate the data behavior. The theorems ensure the convergence of the empirical eigenvalue distributions to deterministic functions as the matrices grow large, which makes the RMT naturally suitable for high-dimensional data analysis. Nowadays, the RMT has been widely used in wireless communication [13], finance [14], quantum information [15], etc. In recent years, some work that makes substantial use of results in the RMT has emerged in the power field. For example, in [16], an architecture with the application of the

This work was partly supported by NSF of China No. 61571296, National Key R & D Program of No. 2018YFF0214705 and (US) NSF Grant No. CNS-1619250.

¹ Department of Electrical Engineering, Center for Big Data and Artificial Intelligence, Shanghai Jiaotong University, Shanghai 200240, China. (e-mail: dugushixin@sjtu.edu.cn; rcqiu@sjtu.edu.cn; hexing_hx@126.com; ling_zenan@163.com; 2457604987@qq.com; leochu@sjtu.edu.cn;)

² Department of Electrical and Computer Engineering, Tennessee Technological University, Cookeville, TN 38505, USA. (e-mail:rcqiu@tntech.edu)

RMT into smart grid is proposed. In [17], based on the RMT, a data-driven approach to reveal the correlations between various factors and the power system status is proposed. In [18] and [19], the RMT is used for power system transient analysis and steady-state analysis, respectively.

In this paper, based on the RMT, a data-driven approach is developed for early anomaly detection and localization in distribution network. It leverages the similarities of the data collected from multiple measurement devices, and reveals the anomaly by tracking the variation of the data correlations. The primary contributions of this paper are shown as follows: 1) The approach is mainly data-driven and it only requires the simple topology information of feeder lines in the distribution network. 2) The approach merges anomaly detection and localization functionalities through analyzing the extreme eigenvalues (outliers) and the corresponding eigenvectors from the data. 3) The approach is sensitive to the variation of the data correlations, and it is capable of detecting and localizing the anomaly at an early stage. 4) It is experimentally validated that the approach is robust against random disturbance and measurement error. 5) An increasing data dimension algorithm is designed, which makes it more accurate for analyzing the low observability feeder lines in the distribution network.

The other sections of this paper are arranged as follows. Section II presents the mathematical foundations of RMT for anomaly detection and localization, in which anomaly indicators are designed and analyzed. In section III, spatio-temporal matrices are formulated by leveraging the measurement data in distribution network and detailed steps of the early anomaly detection and localization approach are presented. Meanwhile, an increasing data dimension algorithm is designed for analyzing the low observability feeders more accurately. In section IV, Both MATPOWER simulation data and real SCADA data are used to verify the feasibility of the developed approach. Conclusions and future research directions are illustrated in Section V.

II. RANDOM MATRIX THEORY FOR ANOMALY DETECTION AND LOCALIZATION

In practical world, massive amounts of data can be naturally represented by large random matrices [20]. In this section, we apply the RMT for anomaly detection and localization of high-dimensional data matrices. First, asymptotic theorem in the RMT is used to analyze the empirical spectral distribution (ESD) of high-dimensional ‘signal+noise’ matrix, and linear statistics of the eigenvalues are introduced as a statistical index to track the data behavior. The details of the RMT for anomaly detection and localization are presented.

A. Asymptotic Theorem for ‘Signal+Noise’ Matrix

Marchenko-Pastur Law (M-P Law): Assume $\mathbf{X} = \{x_{i,j}\} \in \mathbb{C}^{p \times n}$ being a random matrix with independent identically distributed (i.i.d.) entries satisfying: 1) the mean $\mu(x) = 0$ and 2) the variance $\sigma^2(x) < \infty$. The covariance matrix of \mathbf{X} is calculated as $\Sigma = \frac{1}{n} \mathbf{X} \mathbf{X}^H$. According to the M-P law [21],

when $p, n \rightarrow \infty$ and $c = \frac{p}{n} \in (0, 1]$, the ESD of Σ fits to the theoretical limit with probability density function (PDF)

$$f_{MP}(\lambda) = \begin{cases} \frac{1}{2\pi c \sigma^2 \lambda} \sqrt{(b - \lambda)(\lambda - a)}, & a \leq \lambda \leq b \\ 0, & \lambda < a \text{ or } \lambda > b \end{cases}, \quad (1)$$

where $a = \sigma^2(1 - \sqrt{c})^2$, $b = \sigma^2(1 + \sqrt{c})^2$.

We apply the M-P law for a high-dimensional data matrix $\mathbf{X}' \in \mathbb{R}^{p \times n}$. In steady state, \mathbf{X}' is considered to be a random matrix and the ESD of $\Sigma' = \frac{1}{n} \mathbf{X}' \mathbf{X}'^T$ converges to the limiting spectral density $f_{MP}(x')$, as is shown in Figure 1(a). The bars in blue color represent the eigenvalue distributions of Σ' and the M-P law is plotted in the red curve. However, what will happen in unsteady state? Here, “unsteady” means signals occur in \mathbf{X}' and the correlations among the entries x'_{ij} have been changed. Then \mathbf{X}' is considered of the type $\mathbf{X} + \mathbf{P}$, where \mathbf{X} is a random matrix which represents random noise or fluctuations, and \mathbf{P} is a low-rank matrix which represents anomaly signals. Figure 1(b) shows the ESD of Σ' does not converge to the M-P law. It can be observed that the outliers caused by anomaly signals are out of the range $[a, b]$ (i.e., $[0.034, 3.301]$).

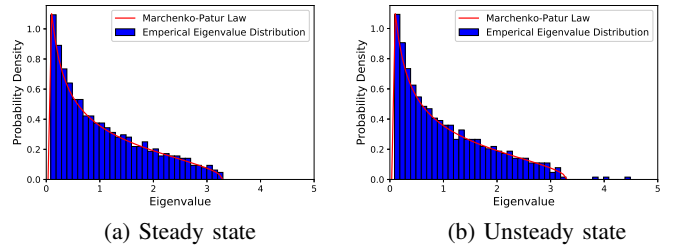


Fig. 1. The empirical spectral density of Σ' and its comparison with the theoretical limit corresponding to steady and unsteady system states, respectively. (a) \mathbf{X}' is a 640×960 random gaussian matrix. (b) $\mathbf{X}' = \mathbf{X} + \mathbf{P}$, where \mathbf{X} is a 640×960 random gaussian matrix, and \mathbf{P} is a low-rank signal matrix.

Based on the analysis above, it can be concluded that the ESDs are different for a high-dimensional random matrix with or without anomaly signals, which inspires us to investigate the statistics regarding the empirical eigenvalues to indicate the data behavior. The linear eigenvalue statistics (LES) via test function ϕ are defined as

$$\mathcal{N}_\phi = \sum_{i=1}^n \phi(\lambda_i), \quad (2)$$

where $\lambda_i (i = 1, 2, \dots, n)$ are the eigenvalues, and the test function ϕ is continuously smooth. The test functions frequently used [20] are listed as follows:

- Chebyshev Polynomial (CP): $\phi(\lambda_i) = a_n + a_{n-1}\lambda_i + \dots + a_0\lambda_i^n$, where $a_k (k = 1, 2, \dots, n)$ are real numbers;
- Information Entropy (IE): $\phi(\lambda_i) = -\lambda_i \ln \lambda_i$;
- Likelihood Ratio Function (LRF): $\phi(\lambda_i) = -1 - \ln \lambda_i + \lambda_i$;
- Wasserstein Distance (WD): $\phi(\lambda_i) = 1 - 2\sqrt{\lambda_i} + \lambda_i$.

The LES constructed via the listed test functions does not introduce any system error, which can be served as an statistical index to track the data behavior. It gives insight into

the data behavior from a high-dimensional perspective, which makes it possible for detecting the latent anomalies in the data. Meanwhile, some statistical properties of the LES have been proved in theory [22], such as satisfying the central limit theorem, with bounded variance, with a fast decay rate (i.e., in the order of $O(p^{-2})$) for the variance, etc.

B. RMT for Anomaly Detection and Localization

Assume there are P -dimensional measurement variables $(x_1, x_2, \dots, x_P) \in \mathbb{R}^P$ for each sampling time. At the sampling time t_j , the P -dimensional measurements can be formulated as a column vector $\mathbf{x}(t_j) = (x_1, x_2, \dots, x_P)^T$. For a series of time N , a data set \mathbf{D} is formulated by arranging these vectors \mathbf{x} in chronological order. Let \mathbf{X} be a $p \times n$ moving window on \mathbf{D} , we can convert it into the standard form $\hat{\mathbf{X}}$ by

$$\hat{x}_{ij} = (x_{ij} - \mu(\mathbf{x}_i)) \times \frac{\sigma(\hat{\mathbf{x}}_i)}{\sigma(\mathbf{x}_i)} + \mu(\hat{\mathbf{x}}_i), \quad (3)$$

where $\mathbf{x}_i = (x_{i1}, x_{i2}, \dots, x_{in})$, $\mu(\hat{\mathbf{x}}_i) = 0$, and $\sigma(\hat{\mathbf{x}}_i) = 1$ ($i = 1, 2, \dots, p; j = 1, 2, \dots, n$). The covariance matrix of $\hat{\mathbf{X}}$ is calculated as $\Sigma = \frac{1}{n} \hat{\mathbf{X}} \hat{\mathbf{X}}^T$. Then the empirical eigenvalues λ_Σ and eigenvectors \mathbf{v}_Σ of Σ can be obtained.

The linear statistics of λ_Σ is calculated through equation (2), which is served as the anomaly detection indicator in the developed approach. Furthermore, the anomaly is located based on the calculated λ_Σ and \mathbf{v}_Σ . According to the definitions on matrix eigenvalue and eigenvector, it can be obtained

$$\Sigma \mathbf{v}_{\Sigma,k} = \lambda_{\Sigma,k} \mathbf{v}_{\Sigma,k}. \quad (4)$$

The derivation of equation (4) regarding the elements ε_{ij} is

$$\frac{d\Sigma}{d\varepsilon_{ij}} \mathbf{v}_{\Sigma,k} + \Sigma \frac{d\mathbf{v}_{\Sigma,k}}{d\varepsilon_{ij}} = \frac{d\lambda_{\Sigma,k}}{d\varepsilon_{ij}} \mathbf{v}_{\Sigma,k} + \lambda_{\Sigma,k} \frac{d\mathbf{v}_{\Sigma,k}}{d\varepsilon_{ij}}. \quad (5)$$

Since Σ is real and symmetric, and there exist $\mathbf{v}_{\Sigma,k}^T \mathbf{v}_{\Sigma,k} = 1$. Left multiply $\mathbf{v}_{\Sigma,k}^T$ for equation (5), we can obtain

$$\frac{d\lambda_{\Sigma,k}}{d\varepsilon_{ij}} = \mathbf{v}_{\Sigma,k}^T \frac{d\Sigma}{d\varepsilon_{ij}} \mathbf{v}_{\Sigma,k}, \quad (6)$$

where

$$\frac{d\Sigma}{d\varepsilon_{ij}} = \begin{cases} 1, & \varepsilon = \varepsilon_{ij} \\ 0, & \varepsilon \neq \varepsilon_{ij} \end{cases}. \quad (7)$$

Thus we can simplify equation (6) as

$$\frac{d\lambda_{\Sigma,k}}{d\varepsilon_{ij}} = v_{\Sigma,k}^{(i)} v_{\Sigma,k}^{(j)}. \quad (8)$$

The contribution rate of the entries in the i th row of Σ to $\lambda_{\Sigma,k}$ can be calculated as

$$\sum_{j=1}^p \left(\frac{d\lambda_{\Sigma,k}}{d\varepsilon_{ij}} \right)^2 = (v_{\Sigma,k}^{(i)})^2 \sum_{j=1}^p (v_{\Sigma,k}^{(j)})^2 = (v_{\Sigma,k}^{(i)})^2. \quad (9)$$

From equation (9), it can be concluded that the i th entry of $\mathbf{v}_{\Sigma,k}$ can be used to measure the ‘‘contribution’’ of the i th row of Σ to $\lambda_{\Sigma,k}$. Based on the analysis of the M-P law for high-dimensional ‘signal+noise’ matrix in Section II-A, it can be observed that outliers (i.e., $\lambda > b$) occur when a system operates in unsteady state. Thus we can realize anomaly localization by analyzing the eigenvectors corresponding to the

outliers. The anomaly localization indicator can be designed as

$$\eta_i = \frac{\sum_{\lambda_{\Sigma,k} \in \{\lambda > b\}} \lambda_{\Sigma,k} (v_{\Sigma,k}^{(i)})^2}{\sum \lambda_{\Sigma,k}}, \quad (10)$$

where $\eta_i \in [0, 1)$. The indicator η_i measures the scale of the i th row’s ‘‘contribution’’ to the anomaly.

We first standardize $\boldsymbol{\eta}$ ($\eta_i \in \boldsymbol{\eta}$) by

$$\hat{\boldsymbol{\eta}} = \frac{\boldsymbol{\eta} - \mu(\boldsymbol{\eta})}{\sigma(\boldsymbol{\eta})}, \quad (11)$$

where $\mu(\boldsymbol{\eta})$ is the mean and $\sigma(\boldsymbol{\eta})$ represents the standard deviation of $\boldsymbol{\eta}$, and $\hat{\boldsymbol{\eta}}$ ($\hat{\eta}_i \in \hat{\boldsymbol{\eta}}$) is the standardized $\boldsymbol{\eta}$. Considering the sample size p of $\hat{\boldsymbol{\eta}}$ is sometimes small, here, $\hat{\boldsymbol{\eta}}$ is assumed to be approximately a t distribution with $p-1$ freedom degree. According to the central limit theorem, the confidence level $1 - \alpha$ for the population mean μ of $\hat{\boldsymbol{\eta}}$ is defined as

$$1 - \alpha = P\left\{ \mu(\hat{\boldsymbol{\eta}}) - t_{\frac{\alpha}{2}} \frac{\sigma(\hat{\boldsymbol{\eta}})}{\sqrt{p}} < \mu < \mu(\hat{\boldsymbol{\eta}}) + t_{\frac{\alpha}{2}} \frac{\sigma(\hat{\boldsymbol{\eta}})}{\sqrt{p}} \right\}, \quad (12)$$

where $\mu(\hat{\boldsymbol{\eta}})$ is the sample mean with $\mu(\hat{\boldsymbol{\eta}}) = 0$ and $\sigma(\hat{\boldsymbol{\eta}})$ is the standard deviation of $\hat{\boldsymbol{\eta}}$ with $\sigma(\hat{\boldsymbol{\eta}}) = 1$, $t_{\frac{\alpha}{2}}$ is the upper $\frac{\alpha}{2}$ critical value for the t distribution, and $P\{\cdot\}$ is the probability operator. For a given $\hat{\eta}_i$, the corresponding confidence level $1 - \alpha$ can be obtained by the t distribution table. For example, let $\hat{\eta}_i = 2.064$ and $p = 25$, then the value of $1 - \alpha$ is calculated to be 95%. Thus, the anomaly can be localized through comparing $1 - \alpha$ with the pre-defined threshold $(1 - \alpha)_{th}$.

In real-time analysis, we can move a window on the formulated data set \mathbf{D} continuously to track the data behavior. Take the current sampling time t_j as an example, the generated data matrix $\mathbf{X}(t_j)$ is written as

$$\mathbf{X}(t_j) = (\mathbf{x}(t_{j-n+1}), \mathbf{x}(t_{j-n+2}), \dots, \mathbf{x}(t_j)), \quad (13)$$

where $\mathbf{x}(t_k) = (x_1, x_2, \dots, x_p)^T$ for $t_{j-n+1} \leq t_k \leq t_j$ represents the measurement data at the sampling time t_k . Thus, the indicator $\mathcal{N}_\phi(t_j)$ and $\boldsymbol{\eta}(t_j)$ can be calculated for the current sampling time t_j .

III. EARLY ANOMALY DETECTION AND LOCALIZATION IN DISTRIBUTION NETWORK

In this section, by leveraging the measurement data collected from the SCADA system installed in distribution network, a RMT-based early anomaly detection and localization approach is developed. First, the measurement data from multiple monitoring devices for each feeder line is formulated as a spatio-temporal data set. Then, detailed steps of the developed approach are presented and advantages of the approach are remarked. Last, an increasing data dimension algorithm is designed for the low observability feeders being more accurately analyzed.

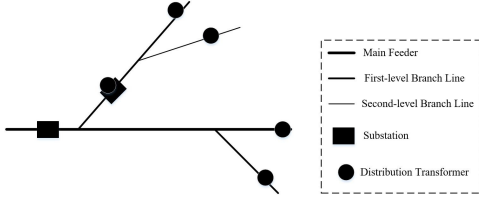


Fig. 2. Circuitry topology diagram of partial distribution network.

A. Formulation of Measurement Data as Spatio-Temporal Matrices

Figure 2 illustrates circuitry topology diagram of partial distribution network, in which a feeder line consists of different level of branch lines and substations with distribution transformers. Multiple online monitoring devices are installed at different physical locations of the feeder, through which we can obtain many types of measurement variables, such as three-phase voltage (u_a, u_b, u_c), three-phase current (i_a, i_b, i_c), active load (l), etc. Here, 7 measurements ($u_a, u_b, u_c, i_a, i_b, i_c, l$) at the sampling time t_j are chosen as the elements to formulate a data vector $\mathbf{d}(t_j) = [u_{aj}^{(1)}, u_{bj}^{(1)}, u_{cj}^{(1)}, i_{aj}^{(1)}, i_{bj}^{(1)}, i_{cj}^{(1)}, l_j^{(1)}, \dots, l_j^{(m)}]^T$, where m denotes the number of monitoring devices and $u_{aj}^{(k)}, u_{bj}^{(k)}, u_{cj}^{(k)}, i_{aj}^{(k)}, i_{bj}^{(k)}, i_{cj}^{(k)}$ ($k = 1, \dots, m$) are the root mean square (RMS) values. Assume $P = 7m$, for a series of time N , we can obtain the data set $\mathbf{D} = [\mathbf{d}(t_1), \mathbf{d}(t_2), \dots, \mathbf{d}(t_N)] \in \mathbb{R}^{P \times N}$. It is noted that, by stacking the measurements together, the formulated spatio-temporal data set contains rich information on the feeder operating states.

B. Early Anomaly Detection and Localization

Based on the work above, we develop a new approach for early anomaly detection and localization in distribution network. The specific steps are given in Table I.

TABLE I

Steps of the RMT for early anomaly Detection and Localization in Distribution Network
1: A spatio-temporal data set $\mathbf{D} \in \mathbb{R}^{P \times N}$ is formulated for every feeder by arranging P measurements in a series of time N .
2: At the sampling time t_j :
2a) Form the data matrix $\mathbf{X}(t_j)$ by using a $p \times n$ ($p = P, n < N$) window on \mathbf{D} ;
2b) Convert $\mathbf{X}(t_j)$ into the standard form matrix $\hat{\mathbf{X}}(t_j)$ through equation (3);
2c) Calculate the sample covariance matrix of $\hat{\mathbf{X}}(t_j)$, i.e., $\Sigma(t_j)$;
2d) Obtain the eigenvalues $\lambda_{\Sigma}(t_j)$ and eigenvectors $\mathbf{v}_{\Sigma}(t_j)$, and compare the ESD with the theoretical limits;
2e) Calculate the linear statistics of $\lambda_{\Sigma}(t_j)$ through equation (2), i.e., $\mathcal{N}_{\phi}(t_j)$;
2f) Calculate the localization indicator $\eta(t_j)$ by using equation (10).
3: Plot the $\mathcal{N}_{\phi} - t$ curve for every feeder during a period of time N .
4: Plot the 3D graph of η regarding the P measurements and time N , and calculate the value of $1 - \alpha$ for every point of the graph to localize the anomaly indexes.

The early anomaly detection and localization approach is driven by the measurement data from SCADA system installed

in distribution network. It is sensitive to the variation of the data correlations, and it is capable of detecting and localizing the anomaly at an early stage. The steps above involve no mechanism models, thus avoiding the errors brought by assumptions and simplifications. The approach merges anomaly detection and localization functionalities, and experimentally robust to random disturbance and measurement error of the data. The computational time of the approach is mainly determined by the calculation of covariance matrix and eigenvalue in Step 2c and 2d, complexity of which approximates $O(p^2 n^2)$. In practice, the covariance matrix and eigenvalue calculation can be implemented by using `numpy.cov()` and `numpy.linalg.eig()` functions in Python, which has an extremely fast computing rate. Therefore, the approach is practical for both online and offline analysis.

C. Discussion

We may notice that the M-P law holds when the data dimensions are infinite or large. However, in the application of early anomaly detection and localization in distribution network, there exist some low observability feeders. Dimensions of the formulated data matrices corresponding to those feeders are often moderate, such as tens or less. In [23] and [24], a natural way of increasing dimensions of data vectors based on tensor product is introduced. On this basis, here, an algorithm to increase the dimensions of data matrices is designed. The algorithm allows for the analysis of high-dimensional data matrices and yields smaller variance for the related functionals.

Assume $\mathbf{X} = [\mathbf{x}_1, \mathbf{x}_2, \dots, \mathbf{x}_t] \in \mathbb{C}^{p \times t}$ be a random matrix with i.i.d. entries, $p = kn$. For $k, t, n \in \mathbb{N}$, we construct a new random vector by using the tensor product of the column vectors of \mathbf{X} in the form

$$\tilde{\mathbf{x}}_j = \mathbf{x}_j^{(1)} \otimes \dots \otimes \mathbf{x}_j^{(k)} \in (\mathbb{C}^n)^{\otimes k}, \quad (14)$$

where $\mathbf{x}_j^{(l)}$ ($j = 1, 2, \dots, n; l = 1, 2, \dots, k$) are i.i.d. copies of a normalized isotropic random vector $\mathbf{x}_j^{(1)} = (x_{1j}, \dots, x_{nj}) \in \mathbb{C}^n$, and ‘ \otimes ’ denotes the tensor product operation. Here, ‘isotropic’ indicates the vectors have the same mean and variance. The new random vector $\tilde{\mathbf{x}}_j$ lies in the n^k dimensional normed space. Thus, the corresponding dimension increased random matrix $\tilde{\mathbf{X}} = [\tilde{\mathbf{x}}_1, \tilde{\mathbf{x}}_2, \dots, \tilde{\mathbf{x}}_t] \in \mathbb{C}^{n^k \times t}$ is obtained. The time and space complexity of the algorithm are $O(kt)$ and $O(n^k)$.

Now consider $n^k \times n^k$ random matrices of the form

$$\mathcal{M}_{n,t,k}(\mathbf{x}) = \sum_{\alpha=1}^t \tau_{\alpha} \tilde{\mathbf{x}}_{\alpha} \tilde{\mathbf{x}}_{\alpha}^H, \quad (15)$$

where τ_{α} ($\alpha = 1, 2, \dots, t$) are real numbers. The asymptotic behavior of $\mathcal{M}_{n,t,k}(\mathbf{x})$ has been well studied in [25]. For every fixed $k \geq 1$, as $t \rightarrow \infty, n \rightarrow \infty$, but $\frac{t}{n^k} \rightarrow c \in (0, \infty)$, the ESD of $\mathcal{M}_{n,t,k}(\mathbf{x})$ converges to a non-random measure.

The ESD of the original covariance random matrix and the tensor product version and their comparisons with the theoretical limits are plotted in Figure 3(a) and Figure 3(b), respectively. It can be observed that the ESD of the original covariance random matrix does not fit to the M-P law for the

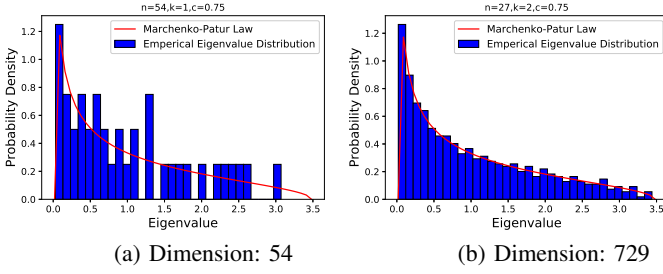


Fig. 3. The ESD of $\mathcal{M}_{n,t,k}(\mathbf{x})$ and its comparison with the M-P law. The dimension of \mathbf{X} is increased from $27 \times 2 = 54$ to $27^2 = 729$ through a tensor product of its column vectors, the ratio c is 0.75, and τ_α is 1.

reason of low dimensions. In contrast, the ESD of the tensor product version of covariance random matrix converges almost surely to the theoretical limits. The increasing data dimension algorithm makes it more accurate for analyzing the formulated data matrices from low observability feeders in the distribution network.

The other issue we want to discuss about the developed approach is that the M-P law holds for the i.i.d. data matrix, which is not true for the measurements collected from a real-world power system. In practice, the collected measurements are correlated whether the system is in steady or unsteady state, and the M-P law does not hold true for them. The differences lie that, the correlations of the measurements corresponding to steady system state are much weaker than that in unsteady state. Thus, the spectrum from the collected measurement data are different when the system operates in steady or unsteady state and the M-P law can be used for depicting the differences, which guarantees the feasibility of the approach for the real data analysis in theory.

IV. CASE STUDIES

In this section, the effectiveness of the developed approach is validated by using both the simulation data generated from standard IEEE test systems [26] and the real measurement data collected from the SCADA system installed in a distribution network. Six cases in different scenarios are designed: 1) In the first four cases, by using the synthetic data, we test the effectiveness of our approach with different test functions, the designed increasing data dimension algorithm, the anomaly localization function and the advantages of the developed approach. 2) The last two cases, leveraging the real measurement data, validate the effectiveness of our approach for analyzing both high and low observability feeders in the distribution network.

A. Case Study with Simulation Data

The simulation data was generated from IEEE 57-bus and 33-bus test systems [26]. The IEEE 33-bus test system is a standard distribution test network and the IEEE 57-bus test system is considered as a distribution network connected to generators. See case57.m and case33.m in Matpower [27] for details. For the generated data \mathbf{D} , a little noise \mathbf{E} was introduced to play the role of random disturbance and measurement error, i.e., $\mathbf{D} = \mathbf{D} + \gamma\mathbf{E}$. The scale of the added

TABLE II
THE ANOMALY SIGNAL SET AT BUS 20 IN CASE 1.

Bus	Sampling Time	Active Load(MW)
20	$t_s = 1 \sim 500$	10
	$t_s = 501 \sim 1000$	12
Others	$t_s = 1 \sim 1000$	Unchanged

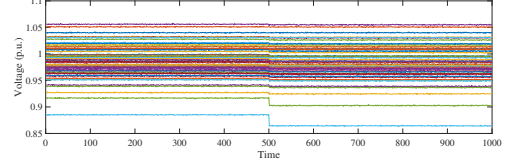


Fig. 4. The generated voltage measurement curves in Case 1.

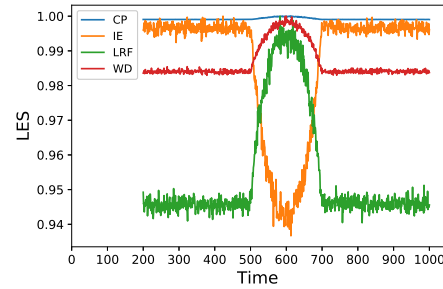


Fig. 5. Effectiveness of the developed approach with different test functions.

noise is $\gamma = \sqrt{\frac{Tr(\mathbf{D}\mathbf{D}^H)}{Tr(\mathbf{E}\mathbf{E}^H) \times \tau_{SNR}}}$, where $Tr()$ represents the trace function and τ_{SNR} is the signal-to-noise ratio. In case 1 and case 2, the white noise was introduced, i.e., $\mathbf{E} \sim N(0, 1)$; in case 3 and case 4, the colored noise was introduced, i.e., $E_{it} = 0.5 * E_{i,t-1} + \varepsilon_{it}$, where $\varepsilon_{it} \sim N(0, 1 - 0.5^2)$ so that the variance of E_t is 1.

1) Case Study on Different Test Functions: In this case, the IEEE 57-bus test system was used to produce the simulation data. For testing the effectiveness of the developed approach with different test functions in equation (2), an anomaly signal was set by changing the active load at bus 20 suddenly, as shown in Table II. The generated data consisted of 57 voltage measurements for a series of 1000 sampling times. The voltage measurement curves were plotted in Figure 4. In the experiment, the moving window's size was 57×200 and τ_{SNR} was set to be 500.

The anomaly detection results of the developed approach with different test functions are normalized into $[0, 1]$, as shown in Figure 5. It is noted that the $\mathcal{N}_\phi - t$ curve begins at $t_s = 200$, because the moving data window consists of 199 historical samples and the current sample. From the $\mathcal{N}_\phi - t$ curves, it can be observed:

I. During $t_s = 200 \sim 500$, \mathcal{N}_ϕ computed through the developed approach with 4 different test functions remain nearly constant, which denotes the system is in steady state. As shown in Figure 6(a), the ESD converges almost surely to the theoretical M-P law.

II. From $t_s = 501$, \mathcal{N}_ϕ begin to change dramatically, which denotes an anomaly occurs. Figure 6(b) shows that

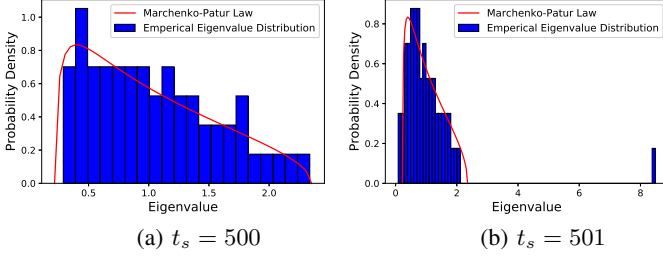


Fig. 6. The ESDs from the voltage measurements and their comparisons with the theoretical M-P law in Case 1.

TABLE III
THE ANOMALY SIGNAL SET FROM BUS 21 TO 22 IN CASE 2.

fBus	tBus	Sampling Time	Impedance(p.u.)
21	22	$t_s = 1 \sim 500$	0.5
		$t_s = 501 \sim 1000$	20
Others	Others	$t_s = 1 \sim 1000$	Unchanged

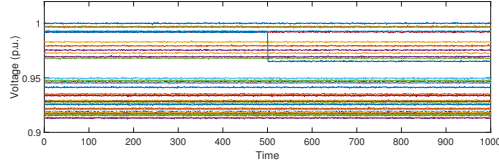


Fig. 7. The generated voltage measurement curves in Case 2.

there exists one outlier, which coincides with the anomaly signal set during the data generation process. It is noted that, from $t_s = 501 \sim 700$, the $\mathcal{N}_\phi - t$ curves are almost U-shaped or inverted U-shaped, because the data window is moved continuously and the duration of the anomaly signal on \mathcal{N}_ϕ is determined by the window width. What's more, the $\mathcal{N}_\phi - t$ curve corresponding to test function IE has the highest variance ratio, which indicates the anomaly indicator via test function IE is more sensitive to the abnormal data behavior. Hence IE was chosen as the test function in subsequent cases.

2) Case Study on Increasing Data Dimension: In this case, the effectiveness of the designed increasing data dimension algorithm was tested. The IEEE 33-bus test system was used to produce the simulation data. During the simulation, an anomaly signal was set by increasing the impedance from bus 21 to 22 suddenly, as shown in Table III. The generated simulation data consisted of 33 voltage measurements for a series of 1000 sampling times. The voltage measurement curves were plotted in Figure 7. In the experiment, the moving window's size was 33×200 , the parameter τ_α in equation (15) was 1, and the signal-to-noise ratio τ_{SNR} defined in Case 1 was set as 500. By using the designed increasing data dimension algorithm, the dimension of each data window was increased from $33 = 16 + 17$ to $272 = 16 \times 17$.

Figure 8(a) and 8(b) show the anomaly detection results corresponding to different data dimensions. From the $\mathcal{N}_\phi - t$ curves, it can be obtained:

I. During $t_s = 200 \sim 500$, the values of \mathcal{N}_ϕ remain almost at 3.33, 4.76, respectively, which denotes the system is in

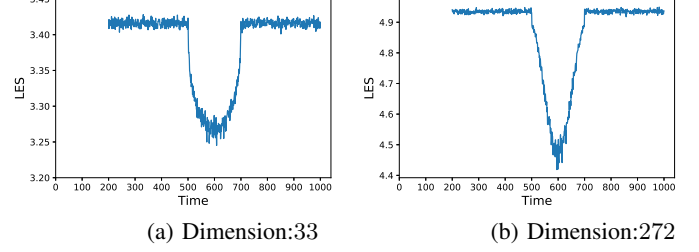


Fig. 8. The anomaly detection results corresponding to different data dimensions. The dimension of the data was increased from 33 to 272.

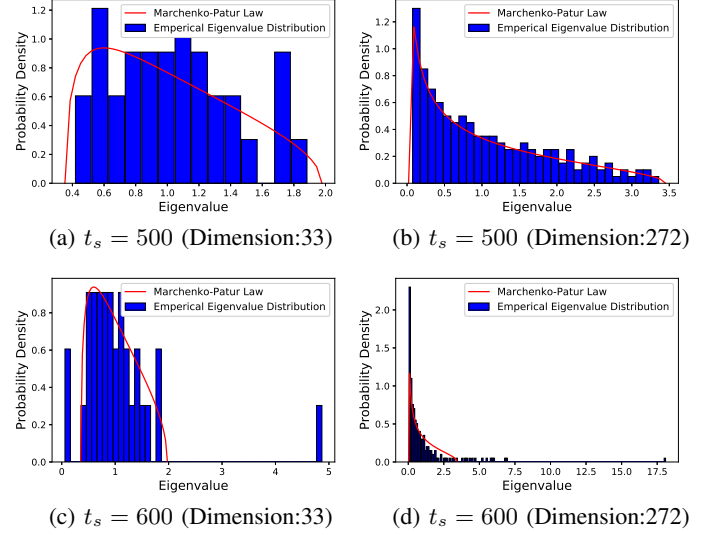


Fig. 9. The ESDs from the voltage measurements and their comparisons with the theoretical M-P law in Case 2.

steady state. The ESD does not fit to the theoretical M-P law in Figure 9(a) for the reason of low data dimension. In contrast, as shown in Figure 9(b), the ESD converges almost surely to the theoretical limit after the data's dimension is increased from 33 to 272.

II. From $t_s = 501$, the $\mathcal{N}_\phi - t$ curves begin to change dramatically, which denotes an anomaly signal occurs and the system is in unsteady state. For example, during $t_s = 501 \sim 600$, the values of \mathcal{N}_ϕ reduce almost from 3.32, 4.75 to 3.10, 2.80, respectively. The ESD does not fit the theoretical M-P law for the reason of existing outliers, as shown in Figure 9(c) and 9(d). The differences lie that more outliers occur and the maximum outlier value becomes larger when the data's dimension is increased from 33 to 272, which makes it much easier to detect the anomaly behavior of the data. What's more, the $\mathcal{N}_\phi - t$ curve corresponding to high data dimension is smoother, which indicates the designed increasing data dimension algorithm can help improve the approach's robustness against random disturbance and measurement error.

3) Case Study On Anomaly Localization: In this case, the developed anomaly localization approach was tested by using the simulation data generated from IEEE 33-bus system. During the simulation, the anomaly signal was set the same as in Case 2, as shown in Table III. The data consisted of 33 voltage measurements for a series of 1000 sampling times. The

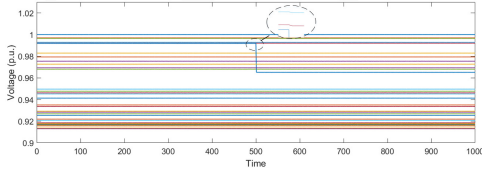


Fig. 10. The voltage measurement curves in Case 3. The anomaly indexes were 20 ~ 22.

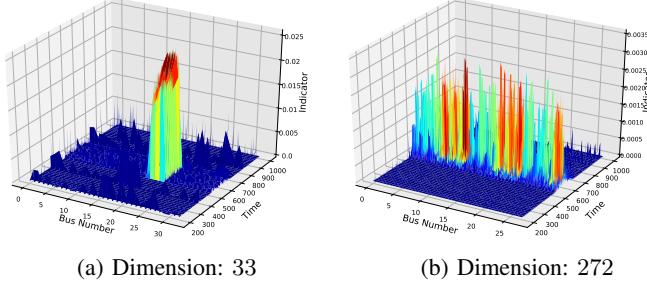


Fig. 11. The anomaly localization results corresponding to different data dimension. The dimension of the data was increased from 33 to 272.

voltage measurement curves with anomaly indexes labelled were plotted in Figure 10. In our experiment, the moving window's size was 33×200 , and the signal-to-noise ratio τ_{SNR} defined in Case 1 was 1000.

Figure 11(a) plots the anomaly localization result. It can be seen that, from $t_s = 501$, the localization indicator $\eta_{20 \sim 22}$ increase dramatically and others stay almost unchanged, which denotes the anomaly occurs on 20 ~ 22 buses. Taking the sampling time $t_s = 501$ as an example, the value of $1 - \alpha$ for bus 20 ~ 22 and other buses (e.g., 23) are 96.65%, 99.59%, 99.91%, and 24.38%, respectively. The localization result coincides with the recorded anomaly indexes.

Furthermore, we explore the effectiveness of the localization approach when the data's dimension is increased from $33 = 16 + 17$ to $272 = 16 \times 17$. Figure 11(b) plots the anomaly localization result. It can be seen that, from $t_s = 501$, the localization indicator $\eta_{3 \sim 5, 20 \sim 22, \dots, 258 \sim 260}$ increase dramatically and others stay almost unchanged. Let $\mathbf{I} = \{3 \sim 5, 20 \sim 22, \dots, 258 \sim 260\}$, at $t_s = 501$, the calculated $1 - \alpha$ corresponding to \mathbf{I} and others (such as 6) are $\{98.84\% \sim 99.50\%, 86.04\% \sim 87.35\%, \dots, 99.63\% \sim 99.77\% \}$ and 44.23%, respectively. Assume $n = 17$, the anomaly location in the original data matrix can be calculated by $\{(\mathbf{I} \bmod n) + n\}$, i.e., $\{20 \sim 22\}$, which coincides with the real anomaly indexes.

4) Case Study on Comparison with Existing Techniques: In this case, we make a comparison on our RMT based approach with SVM [5], AE [11] and LSTM [7] to illustrate the advantage of our approach. The IEEE 57-bus test system was used to produce the simulation data. In the simulation, an anomaly signal was set by increasing the active load of bus 20 gradually, as illustrated in Table IV. The simulation data consisted of 57 voltage measurements for a series of 1000 sampling times, as plotted in Figure 12. In the experiment, the signal-to-noise ratio τ_{SNR} was set as 1000. For SVM, AE or LSTM, a prediction model was firstly trained by using the

TABLE IV
THE ANOMALY SIGNAL SET AT BUS 20 IN CASE 4.

Bus	Sampling Time	Active Load(MW)
20	$t_s = 1 \sim 500$	10
	$t_s = 501 \sim 1000$	10 \rightarrow 60
Others	$t_s = 1 \sim 1000$	Unchanged

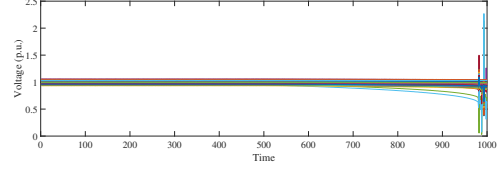


Fig. 12. The generated voltage measurement curves in Case 4.

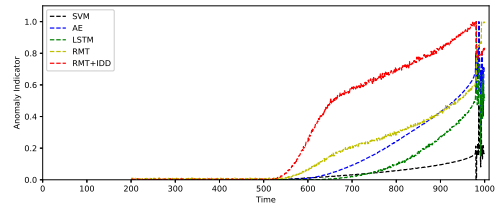


Fig. 13. The comparison result of different anomaly detection techniques in Case 4.

normal data sequence during $t_s = 1 \sim 200$ and calculated the predicting error for the rest sequence during $t_s = 201 \sim 1000$, where the prediction error was considered as the anomaly indicator and each sampling was used as a data sample. The experimental parameters involved in SVM, AE and LSTM can refer Table IV in our previous work [28]. For our approach, both the approach itself (RMT) and its combination with the designed increasing data dimension algorithm (RMT+IDD) were tested. In our approach, the moving window's size was set as 57×200 , the parameter τ_α was 1, and the data's dimension was increased from $57 = 28 + 29$ to $812 = 28 \times 29$.

Figure 13 shows the comparison result of different anomaly detection techniques. For SVM, the normalized value of the signed distance to the separating hyperplane was plotted; for AE and LSTM, the normalization results of the predicting errors were plotted; for RMT and RMT+IDD, $1 - \hat{N}(\phi)$ was plotted, where \hat{N}_ϕ was the normalized form of N_ϕ . It can be observed that, SA+IDD and SA are able to detect the anomaly signal at $t_s = 530 \sim 540$, which is much earlier than the other approaches ($t_s = 610 \sim 630$). It validates that our approach is more sensitive to the abnormal data behavior and it is capable of detecting the anomaly at an early stage. That's because a large moving data window rather than just the current data sample for each sampling time is analyzed in our approach. The average result makes it more robust against random disturbance and measurement error of the data. Moreover, it is noted that RMT+IDD outperforms RMT in anomaly detection, which indicates the designed increasing data dimension algorithm can help improve the sensitivity of RMT approach for abnormal data behavior.

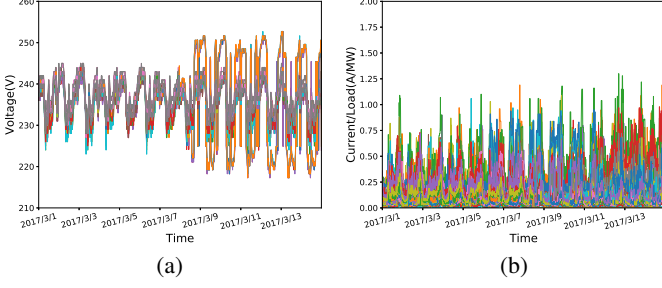


Fig. 14. The measurement data with anomaly time and location indexes recorded in Case 5. (a) Three-phase voltage magnitude curves. (b) Three-phase current and active load magnitude curves. The anomaly time was 2017/3/8 13:45:00 and the anomaly location indexes were 53, 54, 59, 60, 61.

Furthermore, the *average calculating time (ACT)* for each sampling data was counted to compare the efficiency of different detection techniques. For SVM, AE and LSTM, the *ACT* for each data sample in the remaining sequence was calculated, and it did not consist of the model training time. In the experiments, the central processing unit of the computer server was 2.6 GHz, and the random access memory was 8 GB. The *ACT* for SVM, AE, LSTM, RMT and RMT+IDD are 0.001, 0.001, 0.002, 0.002 and 0.029 (unit: s), respectively. Considering the developed approach is an unsupervised approach without any training, it can be concluded that the approach has competitive performance in efficiency.

B. Case Study with Real SCADA Data

The measurement data collected from the SCADA system installed in the distribution network in Hangzhou city of China was used to verify the effectiveness of the developed approach. The distribution network consisted of 200 feeder lines. For every feeder, multiple measurement devices were installed in different physical locations, through which the data was sampled at 15 minute intervals. The anomaly time and location index were recorded during the feeders' operation. In Case 5 and Case 6, three-phase voltage, three-phase current and active load sampled from March 1st, 2017 to March 14th, 2017 were used to form the spatio-temporal data matrices.

5) Case Study on High Observability Feeders: In this case, the developed approach was validated by analyzing a high-dimensional measurement data set from one feeder line. The data was collected from 17 monitoring devices deployed on the feeder and it was consisted of $17 \times 7 = 119$ measurement variables, thus a 119×1344 data set was formed. The measurements with anomaly time and location recorded were plotted in Figure 14. The three-phase voltage curves indicated the anomaly was caused by voltage disturbance (violation). In the experiment, the moving window's size was set as 119×192 . The generated $\mathcal{N}_\phi - t$ curve with continuously moving windows was plotted in Figure 15, in which the anomaly time was marked with a red dashed line. The early anomaly detection process is shown as follows:

I. During 2017/3/3 00:00:00~2017/3/7 22:30:00, \mathcal{N}_ϕ remains nearly constant, which denotes the feeder is in steady state.

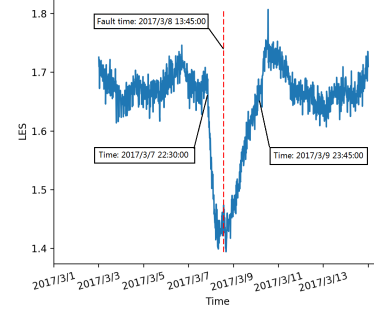


Fig. 15. The anomaly detection result in Case 5.

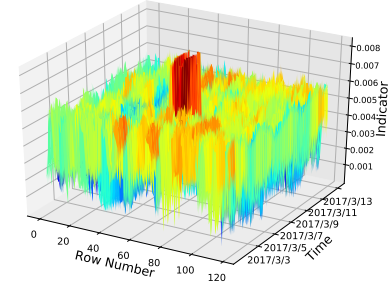


Fig. 16. The anomaly localization result in Case 5.

II. From 2017/3/7 22:30:00, \mathcal{N}_ϕ begins to decrease dramatically, which denotes early anomaly signals occur and the operational state of the feeder begins to deteriorate. In view of the fact that the anomaly time is 2017/3/8 13:45:00, it can be concluded that the anomaly is detected in an early phase by the developed approach. Meanwhile, it is noted that, from 2017/3/7 22:30:00 to 2017/3/9 23:45:00, the $\mathcal{N}_\phi - t$ curve is almost U shaped and the duration of the anomaly signal on \mathcal{N}_ϕ is determined by the window's width, which coincides with our simulation result in Case 1.

Figure 16 is the 3D plot of the localization indicator η regarding 119 measurement variables from 2017/3/3 00:00:00 to 2017/3/14 23:45:00. It can be observed that, from 2017/3/7 22:30:00, $\eta_{\{53,54,59,60,61\}}$ increase rapidly and they are larger than others (such as η_{100}), thus the anomaly index set is determined as $\mathbf{I} = \{53, 54, 59, 60, 61\}$. For example, at 2017/3/7 22:45:00, the calculated values of $1 - \alpha$ corresponding to $\eta_{\mathbf{I}}$ and η_{100} are 99.89%, 99.91%, 99.92%, 99.91%, 99.93% and 34.65%, respectively. The localization result coincides with the recorded anomaly indexes.

6) Case Study on Low Observability Feeders: In this case, the combination of the designed increasing data dimension algorithm and the developed approach was verified by using a low-dimensional measurement data set from one low observability feeder line. The data was collected from 6 monitoring devices and it was consisted of $6 \times 7 = 42$ measurement variables, thus a 42×1344 data set was formed. The measurements with anomaly time and location indexes recorded were plotted in Figure 17. The three-phase current and active load curves demonstrated that the anomaly was caused by overload. In the experiment, the moving window's

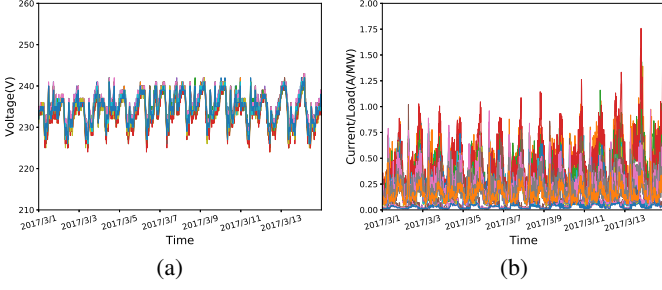


Fig. 17. The measurement data with anomaly time and location indexes recorded in Case 6. (a) Three-phase voltage magnitude curves. (b) Three-phase current and active load magnitude curves. The anomaly time and indexes were 2017/3/8 13:30:00, 2017/3/13 03:00:00 and $\{1, 2, 3\}$, $\{1, 2, 7\}$, respectively.

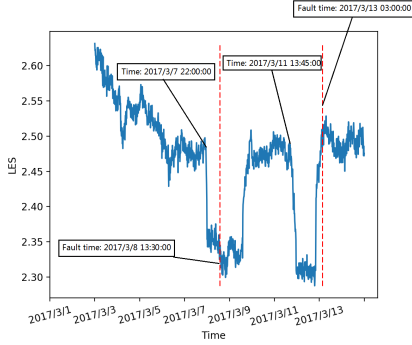


Fig. 18. The anomaly detection result in Case 6.

was set as 42×192 . For each moving data window, the dimension was increased from $42 = 21 \times 2$ to $21^2 = 441$ through the proposed increasing data dimension algorithm, in which τ_α was set as 1. The generated $\mathcal{N}_\phi - t$ curve with continuously moving windows was plotted in Figure 18, in which the anomaly time was marked with red dashed lines. The early anomaly detection process is shown as follows:

I. During 2017/3/3 00:00:00~2017/3/7 22:00:00, \mathcal{N}_ϕ decreases gradually, which indicates the operating state of the feeder is getting worse and the anomaly may occur at any time.

II. From 2017/3/7 22:00:00, \mathcal{N}_ϕ decreases dramatically, which denotes an anomaly signal occurs and the feeder is in unsteady state. In view of the fact that the anomaly time is 2017/3/8 13:30:00, it can be concluded that the anomaly is detected in an early phase. Meanwhile, it is noted that, from 2017/3/7 22:00:00 to 2017/3/9 22:00:00, the $\mathcal{N}_\phi - t$ curve is almost U-shaped and the duration of the anomaly signal on \mathcal{N}_ϕ is determined by the moving window's width, which coincides with the simulation result in Case 1. Similarly, from 2017/3/11 13:45:00, another new anomaly signal is detected, which is much earlier than the recorded anomaly time.

Furthermore, we localized the anomalies through the developed approach, as shown in Figure 19. It can be observed that, from 2017/3/7 22:00:00, $\eta_{1 \sim 63}$ increase rapidly and they are larger than others (such as η_{100}), which indicates the anomaly index set $\mathbf{I} = \{1 \sim 63\}$. For example, at 2017/3/7 22:15:00, the values of $1 - \alpha$ corresponding to $\eta_{\mathbf{I}}$ and η_{100} are $96.74\% \sim 98.91\%$ and 42.32% , respectively. Let $n = 21$, then

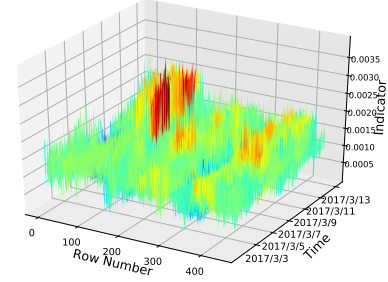


Fig. 19. The anomaly localization result in Case 6.

the anomaly indexes in the original data set can be calculated by $\{\mathbf{I} \bmod n\}$, i.e., $\{1, 2, 3\}$. Similarly, from 2017/3/11 13:45:00, $\eta_{1 \sim 42, 106 \sim 126}$ increase rapidly and they are larger than others (such as η_{200}), which determines the anomaly index set $\mathbf{I}' = \{1 \sim 42, 106 \sim 126\}$. For example, at 2017/3/11 14:00:00, the calculated values of $1 - \alpha$ corresponding to $\eta_{\mathbf{I}'}$ and η_{200} are $99.97\% \sim 99.99\%$, $99.99\% \sim 99.99\%$ and 38.27% , respectively. Then the anomaly indexes in the original data set can be calculated by $\{\mathbf{I}' \bmod n\}$, i.e., $\{1, 2, 7\}$. The localization results coincide with the real anomaly indexes.

V. CONCLUSION

Based on the RMT, a data-driven approach is developed for early anomaly detection and localization in distribution network. It is able to detect and localize the anomaly at an early stage by tracking the variation of the data correlations. The linear eigenvalue statistics give insight into the data behavior from a high-dimensional perspective, which is used as the detection indicator in the developed approach. As for the low observability feeders in the distribution network, an increasing data dimension algorithm is designed for them to be analyzed more accurately. The developed approach is mainly data-driven without requiring complex parameter information of the distribution network. It merges anomaly detection and localization functionalities, and is robust against random disturbance and measurement error. Case studies on the simulation data and the real SCADA data corroborate the feasibility and advantages of the approach.

In our future work, we will focus on two aspects: 1) realizing anomaly declare automatically. Specifically, we will explore an indicator based on the $LES - t$ curve to measure the degree of an anomaly by comparing it with the pre-defined threshold. The optimal threshold value should be searched by a designed algorithm so that the developed approach has a higher detection accuracy rate and a lower false alarming rate for a given data set. 2) realizing the analysis of different types of faults, such as single-phase fault, two-phase fault, three-phase fault, etc. The linear eigenvalue statistics via different test functions are considered as different filters, and we can use them to track different types of fault signals.

REFERENCES

- [1] M. R. Jaafari Mousavi, "Underground distribution cable incipient fault diagnosis system," Ph.D. dissertation, 2007.

- [2] S. Sarri, L. Zanni, M. Popovic, J. Y. L. Boudec, and M. Paolone, "Performance assessment of linear state estimators using synchrophasor measurements," *IEEE Trans. Instrum. Meas.*, vol. 65, no. 3, pp. 535–548, Mar. 2016.
- [3] F. Aminifar, M. Shahidehpour, M. Fotuhi-Firuzabad, and S. Kamalinia, "Power system dynamic state estimation with synchronized phasor measurements," *IEEE Trans. Instrum. Meas.*, vol. 63, no. 2, pp. 352–363, Feb. 2014.
- [4] B. A. Alcaide-Moreno, C. R. Fuerte-Esquivel, M. Glavic, and T. Van Cutsem, "Electric power network state tracking from multirate measurements," *IEEE Trans. Instrum. Meas.*, vol. 67, no. 1, pp. 33–44, Jan. 2018.
- [5] J. Ma and S. Perkins, "Time-series novelty detection using one-class support vector machines," *Proc. IJCNN*, pp. 1741–1745, 2003.
- [6] L. Xie, Y. Chen, and P. R. Kumar, "Dimensionality reduction of synchrophasor data for early event detection: Linearized analysis," *IEEE Trans. Power Syst.*, vol. 29, no. 6, pp. 2784–2794, Nov. 2014.
- [7] P. Malhotra, L. Vig, G. Shroff, and P. Agarwal, "Long short term memory networks for anomaly detection in time series," *Proc. ESANN*, pp. 89–94, 2015.
- [8] L. Chu, R. C. Qiu, X. He, Z. Ling, and Y. Liu, "Massive streaming pmu data modeling and analytics in smart grid state evaluation based on multiple high-dimensional covariance tests," *IEEE Trans. Big Data*, vol. PP, no. 99, pp. 1–1, Mar. 2016.
- [9] M. Pignati, L. Zanni, P. Romano, R. Cherkaoui, and M. Paolone, "Fault detection and faulted line identification in active distribution networks using synchrophasors-based real-time state estimation," *IEEE Trans. Power Del.*, vol. 32, no. 1, pp. 381–392, Feb. 2017.
- [10] M. Wu and L. Xie, "Online detection of low-quality synchrophasor measurements: A data-driven approach," *IEEE Trans. Power Syst.*, vol. 32, no. 4, pp. 2817–2827, Jul. 2017.
- [11] J. Liu, J. Guo, P. Orlik, M. Shibata, D. Nakahara, S. Mii, and M. Takáč, "Anomaly detection in manufacturing systems using structured neural networks," *13th WCICA*, pp. 175–180, 2018.
- [12] J. Wishart, "The generalised product moment distribution in samples from a normal multivariate population," *Biometrika*, vol. 20, no. 1/2, pp. 32–52, 1928.
- [13] R. C. Qiu, Z. Hu, H. Li, and M. C. Wicks, *Cognitive radio communication and networking: Principles and practice*. Hoboken, NJ, USA: Wiley, 2012.
- [14] N. A. S. B. K. Saad, *Random Matrix Theory with Applications in Statistics and Finance*. Canada: Ottawa, 2013.
- [15] K. Chaitanya, "Random matrix theory approach to quantum mechanics," *arXiv preprint arXiv:1501.06665*, 2015. [Online]. Available: <https://arxiv.org/pdf/1501.06665.pdf>
- [16] X. He, Q. Ai, R. C. Qiu, W. Huang, L. Piao, and H. Liu, "A big data architecture design for smart grids based on random matrix theory," *IEEE Trans. Smart Grid*, vol. 8, no. 2, pp. 674–686, Mar. 2017.
- [17] X. Xu, X. He, Q. Ai, and R. C. Qiu, "A correlation analysis method for power systems based on random matrix theory," *IEEE Trans. Smart Grid*, vol. 8, no. 4, pp. 1811–1820, Jul. 2017.
- [18] W. Liu, D. Zhang, X. Wang, D. Liu, and X. Wu, "Power system transient stability analysis based on random matrix theory," *Proc. CSEE*, vol. 36, no. 18, pp. 4854–4863, Oct. 2016.
- [19] X. Wu, D. Zhang, D. Liu, W. Liu, and C. Deng, "A method for power system steady stability situation assessment based on random matrix theory," *Proc. CSEE*, vol. 36, no. 20, pp. 5414–5420, Dec. 2016.
- [20] R. C. Qiu and M. Wicks, *Cognitive Networked Sensing and Big Data*. New York, NY, USA: Springer, 2014.
- [21] V. A. Marčenko and L. A. Pastur, "Distribution of eigenvalues for some sets of random matrices," *Sbornik: Math*, vol. 1, no. 4, pp. 457–483, 1967.
- [22] M. Shcherbina, "Central limit theorem for linear eigenvalue statistics of the wigner and sample covariance random matrices," *arXiv preprint arXiv:1101.3249*, 2011. [Online]. Available: <https://arxiv.org/pdf/1101.3249.pdf>
- [23] R. C. Qiu, *A Mathematical Introduction to Deep Learning: A Random Matrix Theory Approach*. In preprint, 2018.
- [24] A. Ambainis, A. W. Harrow, and M. B. Hastings, "Random tensor theory: Extending random matrix theory to mixtures of random product states," *Commun. Math. Phys.*, vol. 310, no. 1, pp. 25–74, 2012.
- [25] A. Lytova, "Central limit theorem for linear eigenvalue statistics for a tensor product version of sample covariance matrices," *J. Theor. Prob.*, pp. 1–34, 2017.
- [26] R. D. Zimmerman, C. E. Murillo-Sanchez, and R. J. Thomas, "Matpower: Steady-state operations, planning, and analysis tools for power systems research and education," *IEEE Trans. Power Syst.*, vol. 26, no. 1, pp. 12–19, Feb. 2011.
- [27] R. D. Zimmerman and C. E. Murillo-Sánchez, "Matpower 6.0 users manual," Dec. 2016.
- [28] X. Shi and R. Qiu and Z. Ling and F. Yang and H. Yang and X. He, "Spatio-Temporal Correlation Analysis of Online Monitoring Data for Anomaly Detection and Location in Distribution Networks," *IEEE Trans. Smart Grid*, pp. 1–12, Jul. 2019.